Confinement-Shear Lattice Model for Concrete Damage in Tension and Compression: I. Theory

Gianluca Cusatis[1]; Zdeněk P. Bažant, F.ASCE[2]; and Luigi Cedolin, M.ASCE[3]

Abstract: The mechanical behavior of the mesostructure of concrete is simulated by a three-dimensional lattice connecting the centers of aggregate particles. The model can describe not only tensile cracking and continuous fracture but also the nonlinear uniaxial, biaxial, and triaxial response in compression, including the postpeak softening and strain localization. The particle centers representing the lattice nodes are generated randomly, according to the given grain size distribution, and Delaunay triangulation is used to determine the lattice connections and their effective cross-section areas. The deformations are characterized by the displacement and rotation vectors at the centers of the particles (lattice nodes). The lattice struts connecting the particles transmit not only axial forces but also shear forces, with the shear stiffness exhibiting friction and cohesion. The connection stiffness in tension and shear also depends on the transversal confining stress. The transmission of shear forces between particles is effected without postulating any flexural resistance of the struts. The shear transmission and the confinement sensitivity of lattice connections are the most distinctive features greatly enhancing the modeling capability. The interfacial transition zone of the matrix (cement mortar or paste) is assumed to act approximately in series coupling with the bulk of the matrix. The formulation of a numerical algorithm, verification by test data, and parameter calibration are postponed for the subsequent companion paper.

DOI: 10.1061/(ASCE)0733-9399(2003)129:12(1439)

CE Database subject headings: Concrete; Fractures; Damage; Softening; Lattices; Microstructure; Computer analysis; Nonlinear analysis; Particle interaction; Partcle distribution.

Introduction

Discrete microstructural models for concrete, such as random lattice models or random particle models, have established themselves as a powerful and realistic alternative to the nonlocal continuum models for softening damage and fracturing. Both alternatives possess a material characteristic length, automatically exhibit the size effect and macroscopically nonlocal behavior, and eliminate problems with spurious mesh sensitivity plaguing the local continuum models. Compared to the nonlocal continuum models, the random particle or lattice models have several advantages: (1) various microstructural features, such as the aggregate size distribution, as well as the stress and strain field in the microstructure, can be directly simulated; (2) diverse oriented and localized phenomena, such as frictional slip or opening of a microcrack between two aggregate pieces, can be captured (approximately, of course); and (3) the randomness of the microstructure essentially eliminates a global directional bias in fracture propagation direction. This comes at the cost of greatly increased computational work, which still precludes simulation of even moderately large structures or large laboratory specimens, especially since a realistic lattice model must be three-dimensional.

The existing lattice models (e.g., Bažant et al. 1990; Schlangen and van Mier 1992; Schlangen 1993; van Mier et al. 1994; Jirásek and Bažant 1995a,b; Schlangen 1995) can simulate tensile cracking and mode I fracture propagation quite well. However, if they are calibrated to correctly predict tensile cracking, they overpredict the uniaxial compressive strength, typically, by an order of magnitude, and incorrectly indicate a snapback instead of gradual softening with a finite negative slope. Furthermore, these models yield incorrect failure envelopes for triaxial compressive stress states. For hydrostatic compression and uniaxial compressive strain, these models predict a finite strength limit although no strength limit exists in reality. The fact that these models have so far been mostly two-dimensional, rather than three-dimensional, is only one of the causes of these problems. Generally, the simulation of strength limits and postpeak response in compression is beyond the reach of these classical lattice models.

To overcome all these limitations is the objective of this study. To this end, the following innovative features are introduced:

1. The lattice struts connecting adjacent particles transmit not only axial forces (tension or compression) but also shear forces.
2. The tensile and shear behaviors of the connecting struts are sensitive to the lateral confining pressure in directions orthogonal to the strut.
3. The shear response of the lattice struts exhibits friction and cohesion.

Regarding item 1, it should be noted that shear transmission is

[1]Graduate Student, Dept. of Structural Engineering, Technical Univ. (Politecnico) of Milan, Milan 20133, Italy. E-mail: cusatis@stru.polimi.it

[2]McCormick School Professor and W. P. Murphy Professor of Civil Engineering and Materials Science, Northwestern Univ., Evanston, IL 60208. E-mail: z-bazant@northwestern.edu

[3]Professor of Structural Engineering, Dept. of Structural Engineering, Technical Univ. (Politecnico) of Milan, Milan 20133, Italy. E-mail: cedolin@stru.polimi.it

Note. Associate Editor: Stein Sture. Discussion open until May 1, 2004. Separate discussions must be submitted for individual papers. To extend the closing date by one month, a written request must be filed with the ASCE Managing Editor. The manuscript for this paper was submitted for review and possible publication on August 26, 2002; approved on February 21, 2003. This paper is part of the ***Journal of Engineering Mechanics***, Vol. 129, No. 12, December 1, 2003. ©ASCE, ISSN 0733-9399/2003/12-1439–1448/$18.00.

also obtained in the lattice model of van Mier et al. (1994), but at the cost of treating the lattice struts as beams undergoing flexure. This is an unrealistic artifact. The bending of beams is not characteristic of the physical phenomena in the microstructure.

To achieve shear transmission of the connecting struts (item 1), rotations and nodal displacements transversal to the strut are associated with rigid particles simulating the aggregate pieces (in a manner similar to Zubelewicz and Bažant 1987), and these rotations and displacements are then used to calculate the relative shear displacements in the contact zones between particles.

The calculation of the confining pressure on the connecting struts exploits an analogy with the microplane model, and so does the formulation of the constitutive relation of the strut.

In this paper, only the theoretical formulation will be developed. The subsequent companion paper (Cusatis et al. 2003) will deal with the numerical algorithm and calibration by test data.

Background of Previous Studies

The microstructure of concrete—or, in material science terminology, the mesostructure (the term microstructure being reserved for the scale of cement paste and the finest aggregates)—was numerically simulated in the pioneering studies of Roelfstra et al. (1985), Wittmann et al. (1988), and Roelfstra (1988), who developed a model called *numerical concrete* in which the mortar, the aggregates, and the interface between them are described by many elements much smaller than the aggregate pieces. Similar models were proposed by Lopez et al. (2000). The mesostructure is reproduced by continuum elastic elements, which subdivide the matrix and the aggregate pieces and are connected by nonlinear interface elements (Bažant and Cedolin 1991). These elements represent potential crack lines, and the assumed constitutive law is then a mixed-mode generalization of the cohesive crack model (or Hillerborg's fictitious crack model). Such models, however, still adhere to the classical continuum discretization philosophy, lead to an extremely high number of unknowns, and cannot realistically capture compression behavior.

A computationally less demanding approach is to replace the continuum a priori by a system of discrete elements intended to represent the major aggregate pieces in concrete and their interactions. This can be done by rigid particles, as in the discrete element method (DEM) and the rigid-body spring model (RBSM), or by two-node structural elements such as beam elements, bar elements or, in general, one-dimensional finite elements (lattice models). In this case, the displacements are not smoothly represented but are defined only at particle centers or at lattice nodes.

Particle models in the form of the DEM were first developed to describe the behavior of particulate materials by the interaction of rigid particles in contact. Such models were first formulated for geomaterials. Cundall (1971), Serrano and Rodriguez-Ortiz (1973), Rodriguez-Ortiz (1974), Cundall (1978), and Cundall and Strack (1979) proposed rigid particle models interacting only by friction, to simulate the behavior of granular materials such as sand. Zubelewicz (1980), Zubelewicz (1983), Zubelewicz and Mróz (1983), Plesha and Aifantis (1983), and Zubelewicz and Bažant (1987) studied fracture growth in geomaterials by using particle models with nonzero interfacial tensile strength. In this type of models, the particle interaction law is very simple since the overall behavior is controlled mainly by kinematic restrictions of the particle system (e.g., the grain interlock).

The RBSM (Kawai 1978) has similar features. It subdivides the material domain into rigid elements interconnected by zero-size springs placed along their common boundary segments. Bolander and Saito (1998), Bolander et al. (1999), and Bolander et al. (2000) introduced refinements of this model to simulate concrete fracture, obtaining the subdivision by means of Voronoi tesselation.

Realistic though the kinematics of the simulations of all these models may appear, the quantitative stress–strain (averaged) response is not close enough to the actual behavior of the material. One reason for this shortcoming is that most of these models are two-dimensional, and then the three-dimensional effects are inevitably neglected.

As far as lattice models are concerned, two different approaches can be found in the literature. The classical one, which has its root in the pioneering work of Hrennikoff (1941), replaces the actual material by a truss or frame whose geometry is not related to the actual internal geometry of the material. The element size is chosen by the user and the heterogeneity of the material is taken into account by assigning different properties to the lattice elements according to the real material structure.

Schlangen and van Mier (1992), Schlangen (1993), van Mier et al. (1994), and Schlangen (1995) developed this kind of lattice model to analyze concrete fracture [also van Mier et al. (2002) and Arlsan et al. (2002)]. This model is two-dimensional. Each element of the lattice is a beam element with three degrees of freedom per node. The constitutive relation of each beam is linearly elastic and failure is obtained by removing at each step the elements in which the maximum stress exceeds a certain threshold.

The originally proposed lattice configuration was regular, but later Jirásek and Bažant (1995a,b) and Schlangen (1995) have demonstrated that a regular lattice always impresses a strong bias on the direction of fracture propagation, and that such a bias for the overall crack propagation direction can be avoided only by using a random lattice configuration.

A serious question arises about the dependence of the response on the lattice spacing. Schlangen (1995) has shown that while the crack pattern is not strongly affected by the size of the beams, the load-displacement response is affected in much the same way as the effect of mesh refinement in local strain-softening models—the finer the lattice, the smaller the inelastic displacement and the dissipated energy.

In contrast to the lattice models in which the nodal spacing is a free user's parameter, one can formulate lattice models in which the element size is not a free parameter but is determined by the actual material mesostructure. In these models, the position of the lattice nodes coincides with the centers of aggregates or grains and the geometry of each element reflects the actual inter-element connection. Bažant et al. (1990) formulated this type of lattice model as a pinjointed truss. A more refined model is that of Zubelewicz and Bažant (1987) in which also the shear interaction is considered. Using this approach and assuming a softening behavior for each link, one can obtain a very realistic and objective numerical model, albeit limited to tensile fracture problems.

Configuration and Topology of Random Particle System

The model must simulate the mesostructure of concrete. In particular, the particle distribution must meet the required granulometric distribution of the aggregates of various sizes, as determined by the mix design of concrete. The cement content per unit vol-

ume c (kg/m^3), the aggregate content per unit volume a (kg/m^3) and the sieve curve are the input data.

For a given specimen, with volume V, the total mass of aggregates is $M_a = aV$. The number of aggregate pieces of each characteristic size D_i is $N_i^a = \psi_i M_a/(\rho_a v_i)$ for $i=1,...,N$ where $v_i = \pi D_i^3/6$ = volume of one aggregate piece approximated as a sphere; ψ_i = ratio between the mass of aggregates that have characteristic dimension D_i and the total mass of aggregates; ρ_a = mass density of aggregates, and N = number of characteristic sizes chosen to describe the aggregate distribution. The mass density of aggregates, when unknown, can be computed from water–cement ratio w/c and mass density of cement ρ_c. The volume fractions of cement and water are, respectively $V_c = c/\rho_c$ and $V_w = w/\rho_w$, where w is the specific water content (kg/m^3). The mass density of water, ρ_w, is equal to 1,000 kg/m^3. The mass density of cement, ρ_c, depends slightly on the type of cement and for ordinary Portland cement $\rho_c \approx 3{,}150$ kg/m^3. The specific volume of aggregates is then $V_a = 1 - V_c - V_w$, which gives $\rho_a = a/V_a$. In addition, the volume fraction V_e of entrapped or entrained air, if significant, may have to be included in this equation as well.

Since the consideration of extremely small aggregates would result in a prohibitive computational time, aggregates smaller than a certain limit are omitted. Therefore, any physical phenomena occurring on a smaller scale must be described at the level of the constitutive relation for the interparticle links (connecting struts).

An important aspect of the mesostructure is the randomness of the distribution of aggregate particles. This is generally a complex problem for which sophisticated mathematical theories exist in the literature. In concrete, the aggregate particles are not in contact, and that makes the problem simpler. A straightforward procedure for generating a random particle system (Bažant et al. 1990) may then be used.

A uniform probability distribution for the position of each aggregate particle in the specimen is assumed. Applying a random number generator from a standard computer library, one generates the coordinate triplets defining the positions of the aggregate centers. For each new generated position, it is necessary to check for possible overlaps of the new aggregate particle, with the previously placed particles, and with the boundaries of the specimen.

If an overlap occurs the particle is rejected and a new set of coordinates is generated. The placement process must start from the largest aggregates. After the last aggregate piece of the largest size D_1 has been placed, the aggregate pieces of the next smaller size D_2 are placed, etc., until the last aggregate piece of the smallest size has been placed (Bažant et al. 1990).

To define the aggregate particle interactions, Zubelewicz and Bažant (1987) and Bažant et al. (1990) introduced the concept of influence zone of a particle. Each particle, idealized as a sphere of diameter D_i, is assumed to be surrounded by a spherical influence zone with diameter ζD_i where ζ is an empirical coefficient, $\zeta > 1$. The particles are assumed to interact only if their influence zones overlap. This approach is very efficient and it can be implemented without any difficulty. Nevertheless, as observed in this study, not all the aggregate particles will be properly connected. For example, it can happen that too many small aggregates close to the boundaries remain unconnected and the large aggregates are over-connected. Thus, the influence zone concept leads to a particle system whose connections have a more heterogeneous topology than they should.

In this work, therefore, the interaction of particles is based on Delaunay triangulation, which gives a more realistic topology of connections in the mesostructure, and also leads to a more reasonable distribution of the volume and mass (and stiffness) of mortar among the particle connections. The points describing the positions of the aggregates (obtained according to the aforementioned method of Bažant et al. 1990) serve as the input for the triangulation which gives as the output three-dimensional tetrahedra having the given center points as the vertices and filling all the volume of the specimen. Each ridge of each Delaunay tetrahedron represents a connecting strut between two aggregates, and each strut represents such a ridge.

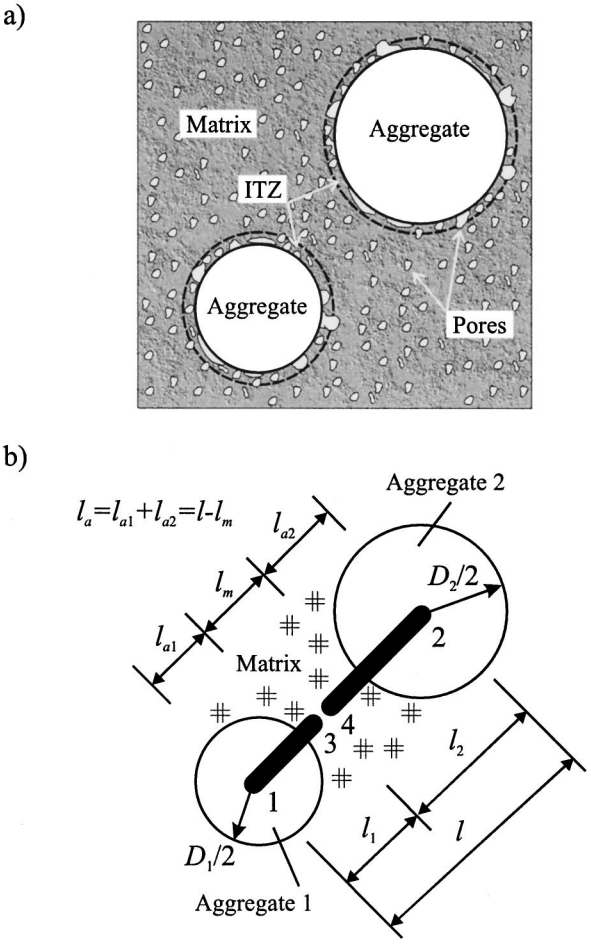

Fig. 1. (a) Interfacial transition zone and (b) geometrical description of the interaction

The cross-sectional area of each connecting strut must be computed so as to preserve the local distribution of the volume. The Delaunay triangulation yields the volume of each tetrahedron which is then distributed among the ridges of that tetrahedron proportionally to their lengths. If Ω^k and p^k, respectively, denote the volume and the sum of the lengths of all the ridges of the generic tetrahedron k ($k=1,...,M$) adjacent to the currently considered connecting strut of length l, then the contribution of that tetrahedron to the volume of the strut is $\Theta^k = \Omega^k l/p^k$. The total volume of a generic connecting strut is the sum of the contributions of all the adjacent tetrahedra whose number is denoted by M. So, the cross-sectional area of the strut is $A = (\Sigma_k \Theta^k)/l = (\Sigma_k \Omega^k l/p^k)/l = \Sigma_k \Omega^k/p^k$, where $k=1,...,M$.

The aggregates are embedded in the matrix of mortar (if the fine aggregates are disregarded) or cement paste (if not). For the sake of simplicity, all the shear deformations of the contact zone of mortar between the particles are considered (similar to

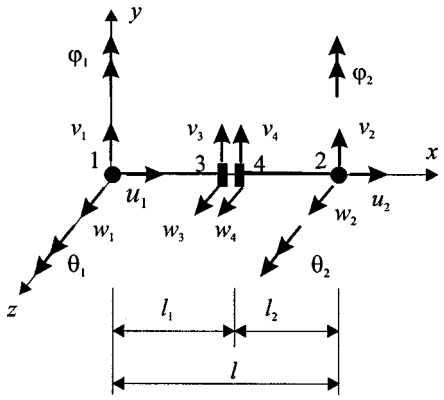

Fig. 2. Current configuration of a connecting strut

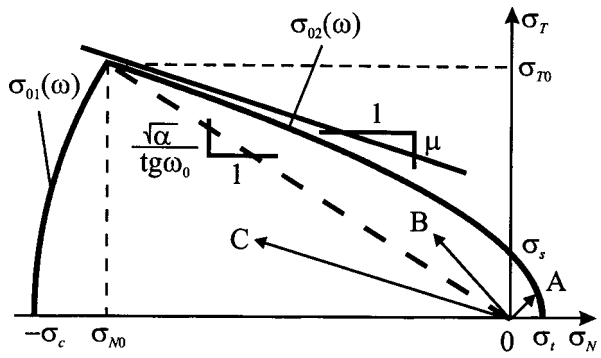

Fig. 3. Elastic domain

Zubelewicz and Bažant 1987) to be lumped into the middle of the contact zone, imagined as the relative displacements between points 3 and 4 in Fig. 1(b), located at distances l_1 and l_2 from the particle centers (lattice nodes); $l_1+l_2=l$, and lengths l_1 and l_2 are assumed to be proportional to the characteristic sizes D_i of the connected aggregates: $l_1=c_1 l$, $l_2=c_2 l$, $c_1=D_1/(D_1+D_2)$, $c_2=D_2/(D_1+D_2)$, and l=distance between the aggregate centers. In this way, each particle is assigned its own random irregular shape. This property is found to be important for a realistic representation of the kinematics of concrete mesostructure, and especially for avoiding excessive rotations of particles, which hampered simulation when regularly shaped particles systems were used (Ting et al. 1995).

On the mesoscale, as is now well understood, the cement mortar (or hardened cement paste) cannot be considered as a homogeneous continuum. Rather, one must recognize that each aggregate particle is surrounded by an interfacial transition zone (ITZ), the properties of which are different from the bulk of mortar. This layer has a certain characteristic thickness δ_l independent of the particle size. Depending on the compactness of aggregate spacing, this layer can occupy different volume fractions of mortar volume. Discretization of the ITZ and of the bulk of mortar obviously does not belong to a mesostructural model and is anyway not computationally feasible since it would increase the number of unknowns by at least three orders of magnitude. So, the interaction of the ITZ with the bulk of mortar must be taken into account in a simplified way, and the following hypothesis is introduced for this purpose. The ITZ and the bulk of mortar interact as two elements coupled in *series* which are in turn coupled in series to the strut portions representing the aggregate particles; see Fig. 1(a). Another simple hypothesis could be a coupling in parallel, but looking at Fig. 1(a) one must immediately recognize it as unrealistic. Summing the compliances of the elements coupled in series, one obtains a single overall compliance of the portion of the strut representing the mortar as a whole, i.e., as a composite of the ITZ and the bulk. This justifies a combined mechanical treatment of the mortar portions in and outside the ITZ.

Axial and Shear Deformation of Connecting Strut

The contact layer of mortar or cement paste matrix between two adjacent aggregate particles can transmit both normal and shear stresses, and so we must consider the interaction of these stresses. We introduce two kinematic assumptions:

1. The axial velocity $\dot{u}$ is linearly distributed between the particle centers [i.e., the strain along the connecting strut 12 (Fig. 2) remains uniform]; and
2. The transversal velocities $\dot{v}$, $\dot{w}$ at the point of contact between two particles are the effect of a rigid-body motion determined by the displacements and angular velocities at center point 1 for side 13, and at center point 2 for side 24.

According to these two assumptions and the sign conventions in Fig. 2, the transversal velocities at points 3 and 4 are $\dot{v}_3=\dot{v}_1+l_1\dot{\vartheta}_1$, $\dot{w}_3=\dot{w}_1-l_1\dot{\varphi}_1$, $\dot{v}_4=\dot{v}_2-l_2\dot{\vartheta}_2$, and $\dot{w}_4=\dot{w}_2+l_2\dot{\varphi}_2$. Because of assumption 1, the rate of axial strain is $\dot{\varepsilon}_N=(\dot{u}_2-\dot{u}_1)/l$. The shear deformation is characterized by the relative displacements between points 3 and 4, which cause shear strains $\dot{\varepsilon}_M$ and $\dot{\varepsilon}_L$ in directions M and L. It will be convenient to use in the constitutive equations the shear strains $\dot{\varepsilon}_M=(\dot{v}_4-\dot{v}_3)/l=(\dot{v}_2-\dot{v}_1-l_2\dot{\vartheta}_2-l_1\dot{\vartheta}_1)/l$ and $\dot{\varepsilon}_L=(\dot{w}_4-\dot{w}_3)/l=(\dot{w}_2-\dot{w}_1+l_2\dot{\varphi}_2+l_1\dot{\varphi}_1)/l$ imagined to be uniformly distributed along the line connecting the particle centers. It might seem more realistic to use $\dot{\varepsilon}_M=(\dot{v}_4-\dot{v}_3)/l_m$ and $\dot{\varepsilon}_L=(\dot{w}_4-\dot{w}_3)/l_m$, where l_m is the width of the contact region between the grains. However, the change from l to l_m is equivalent to changing constitutive parameters by a constant factor, which makes no difference.

To formulate the constitutive law, it is useful to define the following three measures of strain:

$$\varepsilon_T=\sqrt{\varepsilon_M^2+\varepsilon_L^2},\quad \varepsilon=\sqrt{\varepsilon_N^2+\alpha\varepsilon_T^2},\quad \tan\omega=\frac{\varepsilon_N}{\sqrt{\alpha}\varepsilon_T} \tag{1}$$

where ε_T=*total shear strain*. The strain ε, called the *effective strain*, is similar to the strain measure used in the interface element model of Camacho and Ortiz (1996) (also used by Pandolfi et al. 1999); it gives a global measure of the material straining. The strain ω, a new concept introduced in this study, characterizes the degree of coupling between the normal and shear strains and may be called the *coupling strain*. As will be seen, ω is important for reproducing the nonsymmetric character of concrete behavior and for simulating friction. Parameter α is a dimensionless material property used to control the overall Poisson's ratio, as shown later.

The stress σ_T conjugate to ε_T can be computed by applying to shear components the principle of virtual power. The virtual power computed from σ_T, $\dot{\varepsilon}_T$ must be equal to that computed from σ_M, $\dot{\varepsilon}_M$, and σ_L, $\dot{\varepsilon}_L$ for all possible $\dot{\varepsilon}_M$ and $\dot{\varepsilon}_L$. Therefore, $\sigma_T\dot{\varepsilon}_T=\sigma_M\dot{\varepsilon}_M+\sigma_L\dot{\varepsilon}_L$, and because $\dot{\varepsilon}_T=(\varepsilon_M\dot{\varepsilon}_M+\varepsilon_L\dot{\varepsilon}_L)/\varepsilon_T$, we get the relations

$$\sigma_M=\sigma_T\frac{\varepsilon_M}{\varepsilon_T};\quad \sigma_L=\sigma_T\frac{\varepsilon_L}{\varepsilon_T} \tag{2}$$

From Eq. (2), recalling the definition of ε_T, we further obtain $\sigma_T=\sqrt{\sigma_M^2+\sigma_L^2}$, which represents the total shear stress.

In the same way, we can also relate the stresses σ and τ conjugate to ε and ω to the normal and shear stresses. They must satisfy the principle of virtual power which, in this case, reads $\sigma\dot{\varepsilon}+\tau\dot{\omega}=\sigma_N\dot{\varepsilon}_N+\sigma_T\dot{\varepsilon}_T \forall \dot{\varepsilon}_N, \dot{\varepsilon}_T$. From Eq. (1), we can compute the time derivative of ε and ω, $\dot{\varepsilon}=(\varepsilon_N\dot{\varepsilon}_N+\alpha\varepsilon_T\dot{\varepsilon}_T)/\varepsilon$ and $\dot{\omega}=\cos^2\omega(\varepsilon_T\dot{\varepsilon}_N-\varepsilon_N\dot{\varepsilon}_T)/(\varepsilon_T^2\sqrt{\alpha})$. For $\dot{\varepsilon}_N\neq 0$, $\dot{\varepsilon}_T=0$, we have $\dot{\varepsilon}=\varepsilon_N\dot{\varepsilon}_N/\varepsilon$ and $\dot{\omega}=\cos^2\omega\dot{\varepsilon}_N/(\sqrt{\alpha}\varepsilon_T)$, and so

$$\sigma_N=\sigma\frac{\varepsilon_N}{\varepsilon}+\tau\frac{\cos^2\omega}{\sqrt{\alpha}\varepsilon_T} \tag{3}$$

For $\dot{\varepsilon}_T\neq 0$, $\dot{\varepsilon}_N=0$, we have $\dot{\varepsilon}=\alpha\varepsilon_T\dot{\varepsilon}_T/\varepsilon$ and $\dot{\omega}=-\cos^2\omega\varepsilon_N\dot{\varepsilon}_N/(\sqrt{\alpha}\varepsilon_T^2)$, and so

$$\sigma_T=\sigma\frac{\alpha\varepsilon_T}{\varepsilon}-\tau\frac{\cos^2\omega}{\sqrt{\alpha}\varepsilon_T}\frac{\varepsilon_N}{\varepsilon_T} \tag{4}$$

Eqs. (2), (3), and (4) can be used to derive the normal stress σ_N and the tangential stresses σ_M, σ_L from the stresses σ and τ conjugate to ε and ω, respectively.

Having defined σ and τ, we can now state the constitutive relation in terms of the conjugate pairs $\sigma-\varepsilon$ and $\tau-\omega$ instead of $\sigma_N-\varepsilon_N$, $\sigma_M-\varepsilon_M$, and $\sigma_L-\varepsilon_L$. The constitutive relation is given by the functions $\sigma=\sigma(\varepsilon,\omega)$ and $\tau=\tau(\varepsilon,\omega)$. In this study we assume $\tau(\varepsilon,\omega)\equiv 0$. This assumption does not reduce significantly the generality of the formulation. Both the shear and normal stresses are still present in the connecting strut, and a number of useful consequences arise:

1. The material is characterized by a simple constitutive equation, $\sigma=\sigma(\varepsilon,\omega)$.
2. For $\tau\equiv 0$, and taking Eqs. (2), (3), and (4) into account, we get

$$\sigma_N=\sigma\frac{\varepsilon_N}{\varepsilon};\quad \sigma_M=\sigma\frac{\alpha\varepsilon_M}{\varepsilon};\quad \sigma_L=\sigma\frac{\alpha\varepsilon_L}{\varepsilon} \tag{5}$$

   which relate normal and shear stresses to normal and shear strains in a way similar to simple damage models.
3. Taking Eq. (5) into account, we can now define the *effective stress* σ in terms of normal and tangential stresses;

$$\sigma=\sqrt{\sigma_N^2+\frac{\sigma_T^2}{\alpha}} \tag{6}$$

4. By solving (3) and (4) for τ, we get, in general, $\tau=\sqrt{\alpha}\varepsilon_T\sigma_N-\varepsilon_N\sigma_T/\sqrt{\alpha}$, which, for $\tau=0$, becomes $\sqrt{\alpha}\varepsilon_T\sigma_N-\varepsilon_N\sigma_T/\sqrt{\alpha}=0$ or $\varepsilon_N/(\sqrt{\alpha}\varepsilon_T)=\sigma_N/(\sigma_T/\sqrt{\alpha})$.

Since $\varepsilon_N/(\sqrt{\alpha}\varepsilon_T)$ is exactly the definition of $\tan\omega$, we can also write

$$\tan\omega=\frac{\sigma_N}{\sigma_T/\sqrt{\alpha}} \tag{7}$$

which means that the *coupling strain* ω can be expressed as a ratio of the normal and shear components of not only strain but also stress. This is a useful result which will tremendously simplify the formulation of frictional behavior.

Elastic Behavior

The behavior of the material is initially elastic, i.e., $\sigma=E\varepsilon$, where E is the effective elastic modulus of the connecting struts on the microlevel, depending on the elastic properties of the aggregates and the matrix (cement paste or mortar), and on the portions l_a and l_m of the length of the strut, which belong to aggregates and matrix, respectively [Fig. 1(b)]. Assuming a series coupling, we can write $E=l/(l_a/E_a+l_m/E_m)$, where E_a and E_m are related to the Young's moduli of aggregates and matrix, respectively. According to Eq. (5) the elastic relations in terms of normal stress and shear stresses may be written as $\sigma_N=E\varepsilon_N=E_N\varepsilon_N$, $\sigma_M=\alpha E\varepsilon_M=E_T\varepsilon_M$, and $\sigma_L=\alpha E\varepsilon_L=E_T\varepsilon_L$. These relations also show the physical meaning of coefficient α $(=E_T/E_N)$, which controls the Poisson ratio.

Referring to the preceding discussion of the ITZ, it should again be noted that the compliance $1/E_m$ must be understood as the sum of the compliances of the portions of the strut corresponding to the ITZ and the bulk of mortar or cement paste. Knowing their separate mechanical properties and the thickness of the ITZ, one could in principle predict the effective value of $1/E_m$, but such detailed information is not available at present.

Inelastic Behavior

The inelastic behavior is formulated by exploiting the experience with the microplane model. Based on this experience, we use the concept of stress–strain boundary (or strain-dependent yield limit) introduced by Bažant et al. (1996) for the microplane model M3 and used again for microplane models M4 and M5 (Bažant et al. 2000a,b; Caner and Bažant 2000; Bažant and Caner unpublished, 2003). While the microplane model uses a separate boundary for each stress–strain pair, only one boundary is introduced here, imposed on the equivalent stress σ. This boundary, which characterizes both strain-softening damage and strain-hardening compressive behavior, is assumed to be a function of the effective strain ε and the coupling strain ω. Since the aggregates remain elastic, at least for normal concretes, the nonlinearity arises mainly from the matrix (mortar or cement paste). So, strictly speaking, the boundary should depend only on the part of strain corresponding to the matrix. Our use of the total strain is a simplification which is, nevertheless, acceptable since the elastic deformation of the aggregates is very small in comparison to the linear and nonlinear deformations of the matrix. The same simplification is used in the microplane model.

Without the dependence of the boundary on the coupling strain it would be impossible to reproduce the asymmetric response of concrete in tension and compression, and to simulate friction. At first sight, ω to represent friction may seem inadequate. However, because of Eq. (7), a boundary on the effective stress expressed in terms of ω is equivalent to a curve in the $\sigma_N-\sigma_T$ space, in which frictional properties are characterized.

Leaving the physical justification and interpretation for the next section, we first present the boundary equations. The effective stress σ must satisfy the inequality $0\leqslant\sigma\leqslant\sigma_b(\varepsilon,\omega)$ and the boundary $\sigma_b(\varepsilon,\omega)$ can be expressed as

$$\sigma_b(\varepsilon,\omega)=\sigma_0(\omega)\exp\left\{\frac{K(\omega)}{\sigma_0(\omega)}\langle\varepsilon_1(\varepsilon,\omega)-\varepsilon_0(\omega)\rangle\right\} \tag{8}$$

in which the brackets $\langle\cdot\rangle$ are used in Macaulay sense: $\langle x\rangle=\max\{x,0\}$.

Initial Effective Strength Function $\sigma_0(\omega)$

The initial effective strength function $\sigma_0(\omega)$ has the meaning of a strength limit for the effective stress. Because of Eq. (7), it delimits in the stress space the elastic domain, which is assumed to be a hyperbola with a cap in compression (Fig. 3) and may be expressed as $\sigma_0(\omega)=\sigma_{01}(\omega)$ for $\omega\leqslant\omega_0$ and $\sigma_0(\omega)=\sigma_{02}(\omega)$ for $\omega>\omega_0$. Here ω_0 corresponds to the intersection of the curves

$\sigma_{01}(\omega)$ and $\sigma_{02}(\omega)$ and is defined as $\tan\omega_0=\sigma_{N0}/(\sigma_{T0}/\sqrt{\alpha})$ (Fig. 3). The value ω_0 is related to the angle of internal friction of the material, as will be clarified in the next section.

Function $\sigma_{01}(\omega)$ describes the elastic limit for stress states dominated by compression, and is assumed to be an ellipse in the stress space;

$$\sigma_N^2+\frac{\sigma_T^2}{\beta}=\sigma_c^2 \tag{9}$$

Because of Eqs. (6) and (7) we can express σ_N and σ_T as

$$\sigma_N=\sigma\sin\omega;\quad \sigma_T=\sqrt{\alpha}\sigma\cos\omega \tag{10}$$

If we substitute Eq. (10) into Eq. (9) we get an expression for σ_{01}:

$$\sigma_{01}(\omega)=\frac{\sigma_c}{\sqrt{s^2+\alpha c^2/\beta}} \tag{11}$$

in which we denote, for brevity, $s=\sin\omega$, $c=\cos\omega$.

The hyperbola defining function $\sigma_{02}(\omega)$ in the stress space is given by

$$\sigma_T=\mu\sqrt{(\sigma_N-\sigma_t-\sigma_a)^2-\sigma_a^2} \tag{12}$$

Upon introducing into Eq. (12) the relations (10), we get

$$\sigma_{02}(\omega)=\frac{-(\sigma_t+\sigma_a)s+\sqrt{[(\sigma_t+\sigma_a)s]^2+[\alpha(c/\mu)^2-s^2](\sigma_t+2\sigma_a)\sigma_t}}{\alpha(c/\mu)^2-s^2} \tag{13}$$

in which σ_t=microscopic tensile strength; $-\sigma_c$=microscopic compressive strength; and μ and σ_a=respectively, the slope and the intersection of the hyperbola asymptote with the σ_N axis. Further it is useful to introduce, as a material parameter, the shear strength (or cohesion) σ_s which is the intersection of the hyperbola with the σ_T axis. In this case, σ_a is no longer an independent parameter but is to be evaluated as $\sigma_a=0.5\sigma_t[\sigma_s^2/(\mu\sigma_t)^2-1]$. For $\omega=\omega_1=\arctan(\sqrt{\alpha}/\mu)$, the right-hand side of Eq. (13) is not defined and Eq. (12) gives $\sigma_{02}(\omega_1)=0.5(\sigma_t+2\sigma_a)\sigma_t/[(\sigma_t+\sigma_a)\sin\omega_1]$.

Strength Decay Function $\varepsilon_1(\varepsilon,\omega)$

The strength decay function $\varepsilon_1(\varepsilon,\omega)$ is defined as

$$\varepsilon_1(\varepsilon,\omega)=\begin{cases}\varepsilon & \text{for } \omega\leqslant\omega_0\\ \varepsilon_{\max} & \text{for } \omega>\omega_0\end{cases} \tag{14}$$

where $\varepsilon_{\max}=\sqrt{(\max\varepsilon_N)^2+\alpha(\max\varepsilon_T)^2}$ and $\max\varepsilon_N$ and $\max\varepsilon_T$= the maximum normal strain and the maximum shear strain, respectively, that has been reached up to the current time. Note that, for monotonic loading, if $\omega>0$ ($\varepsilon_N>0$) we have $\max\varepsilon_N=\varepsilon_N$ and $\max\varepsilon_T=\varepsilon_T$, and then $\varepsilon_1(\varepsilon,\omega)$ coincides with the effective strain ε; if $\omega_0<\omega\leqslant 0$, we have $\varepsilon_N\leqslant 0$, and then $\max\varepsilon_N=0$ and $\max\varepsilon_T=\varepsilon_T$, which implies $\varepsilon_1(\varepsilon,\omega)=\sqrt{\alpha}\varepsilon_T$. Basically, $\varepsilon_{\max}$ takes into account the irreversibility of the damage due to fracture at the mesolevel.

Strain Limit Function $\varepsilon_0(\omega)$

The strain limit function $\varepsilon_0(\omega)$ represents the limit of the strain ε_1 at which the boundary is no longer equal to $\sigma_0(\omega)$ but starts to evolve exponentially as a function of $\varepsilon_1-\varepsilon_0$, given by Eq. (8). The evolution is hardening for $\omega\leqslant\omega_0$ and softening for $\omega>\omega_0$. We assume $\varepsilon_0(\omega)$ to be the strain at the elastic limit, $\varepsilon_0(\omega)=\sigma_0(\omega)/E$. For $\omega>0$ and $\omega<\omega_0<0$ (in which case $\varepsilon_1=\varepsilon$), the exponential evolution starts as soon as the elastic limit is reached. However, for $\omega_0<\omega<0$ (in which case $\varepsilon_1=\sqrt{\alpha}\varepsilon_T$), the stress reaches the elastic limit while still $\varepsilon_1<\varepsilon_0$, and then the boundary exhibits a plateau before becoming exponential.

Initial Slope Function K(ω)

The evolution of the boundary is governed by the initial slope $K(\omega)$, which is assumed to be (Fig. 4)

$$K(\omega)=\begin{cases}+K_c-K_c\left(\dfrac{\omega+\pi/2}{\omega_0+\pi/2}\right)^{n_c} & \text{for } \omega\leqslant\omega_0\\ -K_t+K_t\left(\dfrac{\omega-\pi/2}{\omega_0-\pi/2}\right)^{n_t} & \text{for } \omega>\omega_0\end{cases} \tag{15}$$

Eq. (15) gives rise to a behavior that is softening for $\omega=\pi/2$ (pure tension) and that is hardening for $\omega=-\pi/2$ (pure compression).

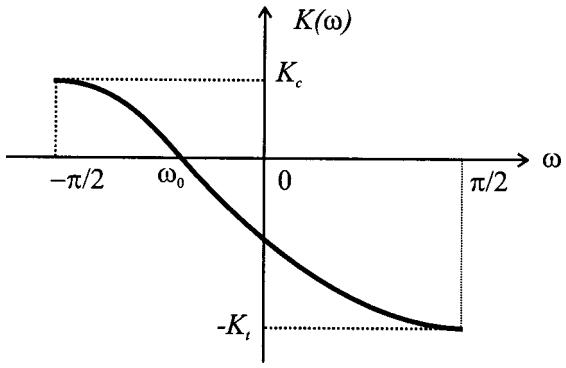

Fig. 4. Initial slope of the stress–strain boundary as a function of ω

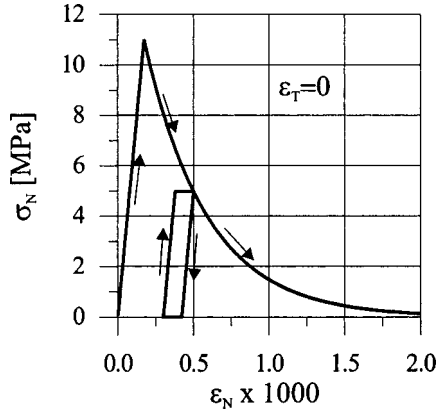

Fig. 5. Response of the connecting strut in pure tension

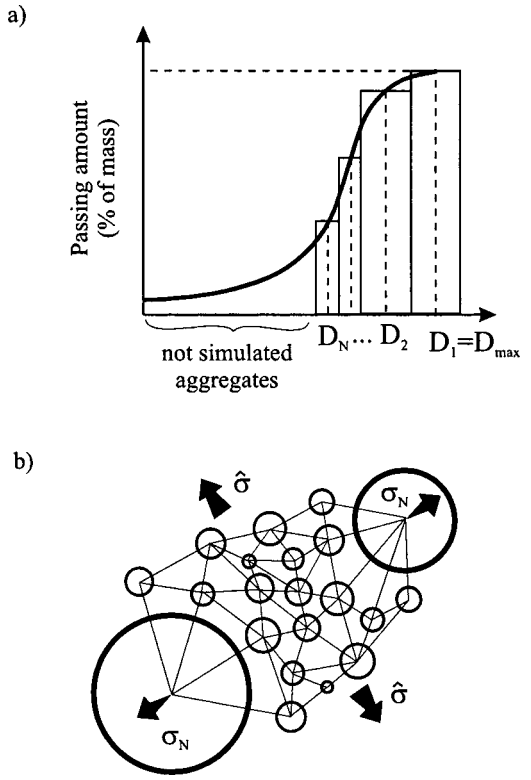

Fig. 6. (a) Sieve curve and (b) mesostructure idealization

In between, there is a regular transition from softening to hardening and the behavior is perfectly plastic for $\omega = \omega_0$.

Constitutive Law with Shear and Confinement Effect

Let us now analyze the model just presented at the level of each connecting strut. For $\varepsilon_T = 0$ ($\sigma_T = 0$) and $\varepsilon_N > 0$ (pure tension at the meso-level), we have $\sigma = \sigma_N$, $\varepsilon_1 = \max \varepsilon_N$, $\varepsilon = \varepsilon_N$, $\omega = \pi/2$, $K(\omega) = -K_t$, $\sigma_0(\omega) = \sigma_t$, $\varepsilon_0(\omega) = \varepsilon_t = \sigma_t / E_N$, and then the governing equations are $\dot{\sigma}_N = E_N \dot{\varepsilon}_N$, $0 \leq \sigma_N \leq \sigma_b^N$, and $\sigma_b^N = \sigma_t \exp\{-K_t \langle \max \varepsilon_N - \varepsilon_t \rangle / \sigma_t\}$. In this case, the model simulates the growth of mode I cohesive fracture between two aggregates. Even at the strut level, the fracturing damage localizes, and so, in order to preserve the correct energy dissipation (Bažant and Oh 1983), we need to impose

$$\int_0^\infty \sigma_N(\varepsilon_N) d\varepsilon_N = G_t / l \tag{16}$$

where G_t=mesoscopic fracture energy; and l=length of the current element. From Eq. (16) one gets

$$K_t = \frac{2E_N}{(l_{cr}/l - 1)} \tag{17}$$

where $l_{cr} = 2E_N G_t / \sigma_t^2$. Assuming $E_m = 50$ GPa, $E_a = 6E_m$, $l_a = 7$ mm, $l = 27.36$ mm, $\sigma_t = 11$ MPa, and $G_t = 0.15$ N/mm, we get the response shown in Fig. 5.

The foregoing relations would suffice to simulate fracture in mode I at the mesolevel if we could reproduce the entire granulometric curve of the material, from the largest aggregate size to the smallest. However, because the computational time would be excessive, we are forced to limit the granulometric curve by choosing a certain lower bound on the aggregate size simulated

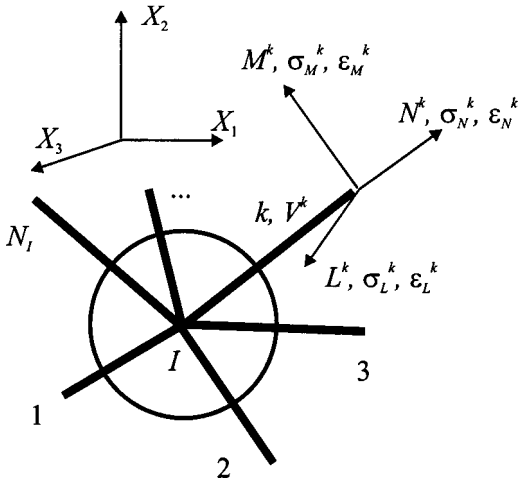

Fig. 7. Aggregate particle connections

[Fig. 6(a)]. This simplification has implications for the confinement effect. If we took into account also the very small aggregates located between two large aggregates, as shown in Fig. 6(b), the interaction between the two large aggregates in the direction of their connecting line would change since it must depend on the transversal confining stresses $\hat{\sigma}$ normal to the connecting strut, which are induced in the contact layer by inclined struts connecting the small aggregates. So, we must keep in mind that the confinement effect depends on the chosen lowest level of discretization. However, to change the confinement effect significantly, it appears that the particle size threshold would have to be decreased by an order of magnitude (which would cause a 1,000-fold increase in the number of particles). This effect would not disappear even if the finest aggregate particles were simulated because confinement is also provided by pure cement paste. For this reason, a pure lattice model (i.e., a truss) is impossible, even in theory.

Aside from the fine particle connections transverse to the strut, the dependence of the $\sigma_N - \varepsilon_N$ relation on $\hat{\sigma}$ is physically also justified by the fact that the frictional pullout resistance of crack-bridging fragments and small aggregate pieces, which is the cause of gradual softening, depends on the confining stresses. Based on the foregoing arguments, Eq. (17) may be replaced by

$$K_t = \frac{2E_N}{(l_{cr}/l - 1)} f(\hat{\sigma}), \quad f(\hat{\sigma}) = 1 + \hat{a} \langle \max \hat{\sigma} \rangle \tag{18}$$

in which $\max \hat{\sigma}$=maximum value of the confining transversal stress $\hat{\sigma}$ reached up to the current time; and $\hat{a}$=material parameter. Note that the present formulation for the normal component of stress is similar to that used in microplane model M4 (Bažant et al. 2000a), in which an exponential softening is assumed and the softening modulus depends on the volumetric stress, which includes the effect of the transversal stress. This analogy helps in figuring out the confining stress $\hat{\sigma}$ for each lattice element. Let us consider an aggregate (I) with its connections as shown in Fig. 7. In analogy to the microplane model, we assume that the strain in each connection is the projection of the strain tensor

$$\varepsilon_N^k = N_{ij}^k \varepsilon_{ij}^I; \quad \varepsilon_M^k = M_{ij}^k \varepsilon_{ij}^I; \quad \varepsilon_L^k = L_{ij}^k \varepsilon_{ij}^I \tag{19}$$

where $N_{ij}^k = n_i^k n_j^k$, $M_{ij}^k = (m_i^k n_j^k + m_j^k n_i^k)/2$, and $L_{ij}^k = (l_i^k n_j^k + l_j^k n_i^k)/2$; n_i=components of the unit vector in the direction of the current connecting strut and l_i, m_i=components of two arbi-

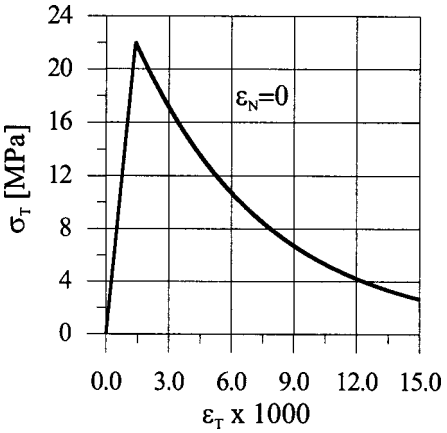

Fig. 8. Response of the connecting strut in pure shear

trarily chosen orthogonal unit vectors lying on a plane orthogonal to the strut (Bažant and Prat 1988).

The stress tensor can be computed by using the principle of virtual power, which requires that the power produced by the stresses acting in the connections equals the power produced by the stress tensor:

$$\sigma_{ij}^I \dot{\varepsilon}_{ij}^I \sum_{k=1}^{N_I} V^k = \sum_{k=1}^{N_I} V^k (\sigma_N^k \dot{\varepsilon}_N^k + \sigma_M^k \dot{\varepsilon}_M^k + \sigma_L^k \dot{\varepsilon}_L^k) \tag{20}$$

where N_I=number of connections of the current aggregate (I in Fig. 7). By using Eqs. (19) and (20) we get

$$\sigma_{ij}^I = \frac{\Sigma_{k=1}^{N_I} V^k (\sigma_N^k N_{ij}^k + \sigma_M^k M_{ij}^k + \sigma_L^k L_{ij}^k)}{\Sigma_{k=1}^{N_I} V^k} \tag{21}$$

Eq. (21) is usable only if at least two connecting struts emanate from each particle center (node), but this condition is satisfied for any lattice coming from Delaunay triangulation in which each particle is a vertex of a tetrahedron. The stress tensor in each connection can be computed by a linear interpolation of the stress tensors computed for the connected nodes $\sigma_{ij}=(l_2\sigma_{ij}^1+l_1\sigma_{ij}^2)/l$.

The components of the stress tensor σ_{ij} refer to a global system of reference. The stress components in the current element local system can be computed as $\sigma_{\alpha\beta}^*=\sigma_{ij}P_{\alpha j}P_{\beta i}$ where P_{ij} is a transformation tensor whose components are the components of the unit vectors of the local system of reference. If we assume that direction x coincides with the direction of the elements, then the confining stress may be defined as the mean transversal normal stress, $\hat{\sigma}=(\sigma_{yy}^*+\sigma_{zz}^*)/2$.

The response in pure shear at the mesolevel is provided by the model once we assume $\varepsilon_N=0$ ($\sigma_N=0$) and $\varepsilon_T>0$. In this case we have $\sigma=\sigma_T/\sqrt{\alpha}$, $\varepsilon_1=\sqrt{\alpha}\max\varepsilon_T$, $\varepsilon=\sqrt{\alpha}\varepsilon_T$, $\omega=0$, $K(\omega)=-K_s/\alpha$, where $K_s=\alpha K_t[1-\{1/(1-2\omega_0/\pi)\}^{n_t}]$, $\sigma_0(\omega)=\sigma_s/\sqrt{\alpha}$, $\varepsilon_0(\omega)=\sqrt{\alpha}\varepsilon_s=\sigma_s/(E_N\sqrt{\alpha})$, and then the governing equations are $\dot{\sigma}_T=E_T\dot{\varepsilon}_T$, $0\leq\sigma_T\leq\sigma_b^T$, and $\sigma_b^T=\sigma_s\exp\{-K_s\langle\max\varepsilon_T-\varepsilon_s\rangle/\sigma_s\}$ in which $E_T=\alpha E_N$. Assuming the same parameters as used in the previous analysis and $\sigma_s=2\sigma_t$, $\alpha=0.25$, and $n_t=2$, we get the response shown in Fig. 8. This response reproduces fracture in mode II at the mesolevel. This response will also depend on the confining stress $\hat{\sigma}$ because the shear softening modulus K_s is proportional to K_t which, in turn, depends on $\hat{\sigma}$.

Note that, for pure shear, the model exhibits no deformation in the direction normal to the shear stress, and thus the phenomenon

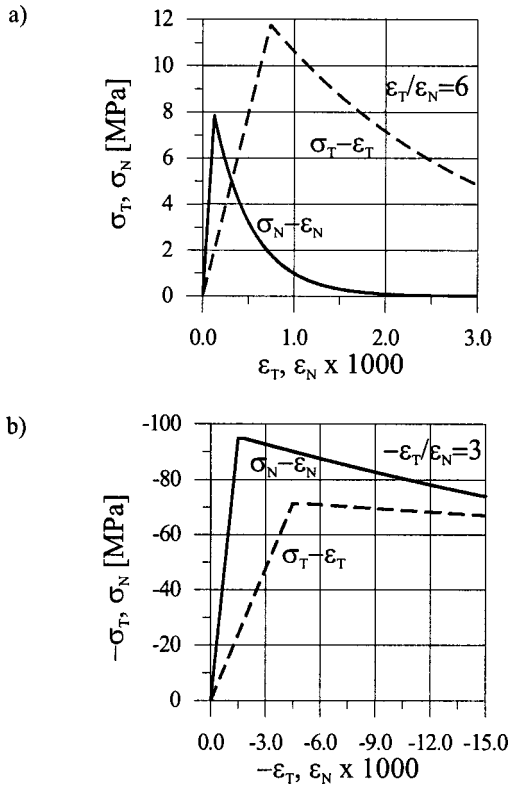

Fig. 9. Response of the connecting strut: (a) tension and shear and (b) shear and low compression

of shear dilatancy does not exist at the mesolevel. Nevertheless, at the macrolevel, shearing of a crack passing through the lattice will exhibit dilatancy because the crack cannot be plane but must contain interlocking segments of different slopes. Since the entire sieve curve cannot be simulated, a certain dilatancy at the level of constitutive relation may be caused by interlocking of very small aggregates not included in the analysis. However, no dilatancy is incorporated into the present constitutive relation since the major source of concrete dilatancy is known to be the coarse aggregate.

The mesoscale parameters must be expected to depend at least to some extent on the threshold at which the sieve curve is terminated. However, characterizing this effect would require extensive simulations which are beyond the scope of this paper. Nevertheless, based on very limited computational experience, it seems that a significant change in response is obtained only by an order-of-magnitude decrease in the threshold, which would cause about a thousand-fold increase in the computational demands.

The ITZ between the aggregates and the cement paste is not simulated directly, as already explained. In keeping with the series coupling hypothesis which allows summing of the elastic compliances, all of inelastic behavior of the ITZ and the bulk of mortar or cement paste is lumped into the constitutive law of the connecting struts between aggregates. The series coupling hypothesis could, in principle, be used to consider the effect of differences in volume fraction of ITZ in cement mortar, but in view of insufficient data this would be mere speculation at present.

Figs. 9(a) and 9(b) represent the response of the model to the loading paths $\overline{0A}$ and $\overline{0B}$ shown in Fig. 3 (with $\mu=0.2$). Path $\overline{0A}$ is a radial path in tension and shear, the response is softening and stresses go asymptotically to zero. Path $\overline{0A}$ is a radial path as well

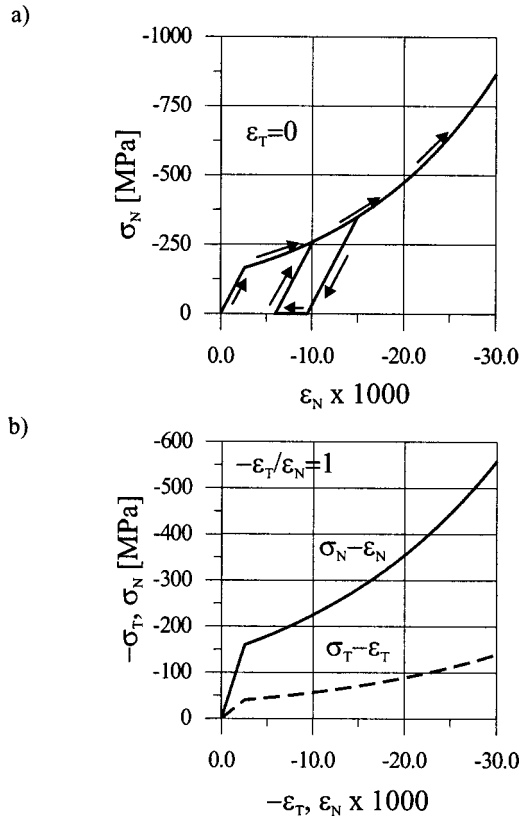

Fig. 10. Response of the connecting strut: (a) pure compression and (b) shear and high compression

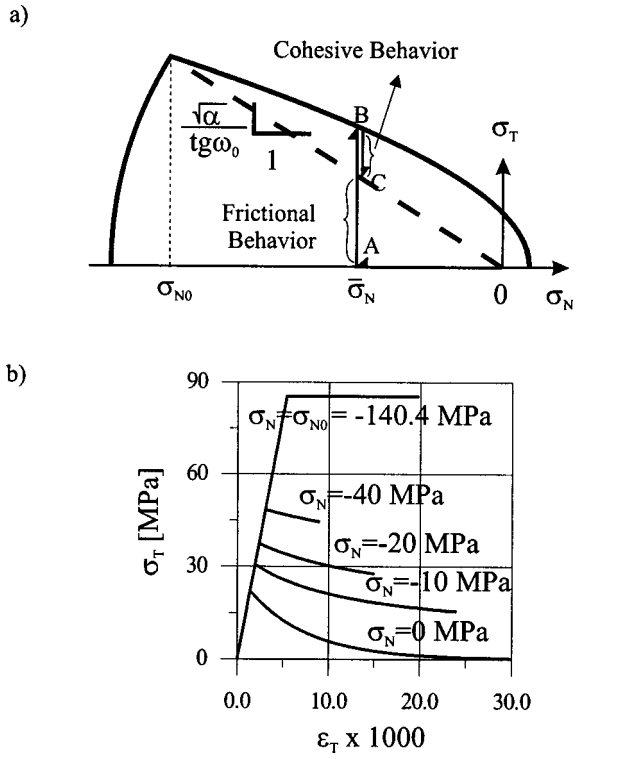

Fig. 11. (a) Loading path in shear at constant compression and (b) response in shear for various compressive stresses

but now shear stress is coupled with a compressive stress. The response is softening but both the peak load and the softening modulus are higher than before.

Let us now consider the case of pure compression at the mesolevel. The phenomena to be reproduced are the crushing of cement paste in compression, which causes a deviation from linearity with a progressive yielding of the material, and the subsequent closure and collapse of pores, which leads to an increase of the hardening modulus. By assuming $\varepsilon_T=0$ ($\sigma_T=0$) and $\varepsilon_N<0$, we have $\sigma=|\sigma_N|$, $\varepsilon_1=\varepsilon=|\varepsilon_N|$, $\omega=-\pi/2$, $K(\omega)=K_c$, $\sigma_0(\omega)=\sigma_c$, $\varepsilon_0(\omega)=\varepsilon_c=\sigma_c/E_N$, and then the governing equations are $\dot{\sigma}_N=E_N\dot{\varepsilon}_N$, $\sigma_b^N\leq\sigma_N\leq 0$, and $\sigma_b^N=-\sigma_c\exp\{K_c\langle-\varepsilon_N-\varepsilon_c\rangle/\sigma_c\}$. The computed response, assuming $\sigma_c=15\sigma_t$ and $K_c=0.2E_m$, is shown in Fig. 10(a). Once, again, we note that the resulting mathematical formulation appears similar to that of microplane models M4 and M5 (Bažant et al. 2000a,b; Bažant and Caner, unpublished, 2003), in which the crushing and pore collapse are modeled by an exponential boundary on the volumetric component.

Fig. 10(b) shows the response of the model (with $n_c=2$, $\beta=1$) to the loading path $\overline{0C}$ represented in Fig. 3. In contrast to loading path $\overline{0B}$ considered before, we now deal with shear at high compressive stress, followed by hardening for both components.

Finally, we analyze the response to the loading path in shear at constant compressive stress, shown in Fig. 11(a). First the normal stress increases in compression without shear [$\overline{0A}$ in Fig. 11(a)], and then the shear strain is increased [$\overline{ABC}$ in Fig. 11(a)] while the normal stress is kept constant ($\sigma_N=\bar{\sigma}_N$). The behavior of the material is elastic until the stress state reaches the elastic domain (point *B*). Afterwards the behavior is softening, but the shear stress does not go to zero; it tends asymptotically to the value $(\sqrt{\alpha}/\tan\omega_0)|\bar{\sigma}_N|$, which represents the frictional limit. In other words, the angle of internal friction displayed by the model is $\varphi_{fr}=\arctan(\sqrt{\alpha}/\tan\omega_0)$. Fig. 11(b) shows the model response for different values of $\bar{\sigma}_N$.

Closing Comment

The material model that has been formulated has various attractive features, which need to be verified in numerical simulations. This task, along with the formulation of conclusions, is relegated to the second part of this study, which follows.

References

Arlsan, A., Ince, R., and Karihaloo, B. L. (2002). "Improved lattice model for concrete fracture." *J. Eng. Mech.*, 128(1), 57–65.

Bažant, Z. P., Caner, F. C., Carol, I., Adley, M. D., and Akers, S. A. (2000a). "Microplane model M4 for concrete. I: Formulation with work-conjugate deviatoric stress." *J. Eng. Mech.*, 126(9), 944–953.

Bažant, Z. P., Caner, F. C., Adley, M. D., and Akers, S. A. (2000b). "Fracturing rate effect and creep in microplane model for dynamics." *J. Eng. Mech.*, 126(9), 962–970.

Bažant, Z. P., and Cedolin, L. (1991). *Stability of structures: Elastic, inelastic, fracture, and damage theories*, Oxford University Press, New York; also 2nd Ed., Dover, New York, 2003.

Bažant, Z. P., and Oh, B. H. (1983). "Crack band theory for fracture of concrete." *Mater. Struct. (Paris)*, 16, 155–177.

Bažant, Z. P., and Prat, P. C. (1988). "Microplane model for brittle plastic material. I: Theory." *J. Eng. Mech.*, 114(10), 1672–1688.

Bažant, Z. P., Tabarra, M. R., Kazemi, T., and Pijaudier-Cabot, G. (1990). "Random particle model for fracture of aggregate or fiber composites." *J. Eng. Mech.*, 116(8), 1686–1705.

Bažant, Z. P., Xiang, Y., and Prat, P. C. (1996). ''Microplane model for concrete. I: Stress–strain boundaries and finite strain.'' *J. Eng. Mech.*, 122(3), 245–254.

Bolander, J. E., Hong, G. S., and Yoshitake, K. (2000). ''Structural concrete analysis using rigid-body-spring networks.'' *J. Comput.-Aided Civil Infrastruct. Eng.*, 15, 120–133.

Bolander, J. E., and Saito, S. (1998). ''Fracture analysis using spring network with random geometry.'' *Eng. Fract. Mech.*, 61(5-6), 569–591.

Bolander, J. E., Yoshitake, K., and Thomure, J. (1999). ''Stress analysis using elastically uniform rigid-body-spring networks.'' *J. Struct. Mech. Earthquake Eng., JSCE*, 633(I-49), 25–32.

Camacho, G. T., and Ortiz, M. (1996). ''Computational modeling of impact damage in brittle materials.'' *Int. J. Solids Struct.*, 33(20-22), 2899–2938.

Caner, F. C., and Bažant, Z. P. (2000). ''Microplane model M4 for concrete. II: Algorithm and calibration.'' *J. Eng. Mech.*, 126(9), 954–961.

Cundall, P. A. (1971). ''A computer model for simulating progressive large scale movements in blocky rock systems.'' *Proc., Int. Symp. Rock Fracture, ISRM*, Nancy, France, 2–8.

Cundall, P. A. (1978). ''BALL—A program to model granular media using distinct element method.'' *Technical note*, Advanced Tech. Group, Dames and Moore, London, U.K.

Cundall, P. A., and Strack, O. D. L. (1979). ''A discrete numerical model for granular assemblies.'' *Geotechnique*, 29, 47–65.

Cusatis, G., Bažant, Z. P., and Cedolin, L. (2003). ''Confinement-shear lattice model for concrete damage in tension and compression: II. Computation and validation.'' *J. Eng. Mech.*, 129(12), 1449–1458.

Hrennikoff, A. (1941). ''Solution of problems of elasticity by the framework method.'' *J. Appl. Mech. Tech. Phys.*, 12, 169–175.

Jirásek, M., and Bažant, Z. P. (1995a). ''Macroscopic fracture characteristics of random particle systems.'' *Int. J. Fract.*, 69(3), 201–228.

Jirásek, M., and Bažant, Z. P. (1995b). ''Particle model for quasibrittle fracture and application to sea ice.'' *J. Eng. Mech.*, 121(9), 1016–1025.

Kawai, T. (1978). ''New discrete models and their application to seismic response analysis of structures.'' *Nucl. Eng. Des.*, 48, 207–229.

Lopez, C. M., Carol, I., and Aguado, A. (2000). ''Microstructural analysis of concrete fracture using interface elements.'' *Proc., European Congress on Computational Methods in Applied Sciences and Eng.*, Barcelona, 1–18.

Pandolfi, A., Krysl, P., and Ortiz, M. (1999). ''Finite element simulation of ring expansion and fragmentation: The capturing of length and time scales through cohesive models.'' *Int. J. Fract.*, 95, 279–297.

Plesha, M. E., and Aifantis, E. C. (1983). ''On the modeling of rocks with microstructure.'' *Proc., 24th U.S. Symp. Rock Mech.*, Texas A & M Univ., College Station, Tex., 27–39.

Rodriguez-Ortiz, J. M. (1974). ''Study of behavior of granular heterogeneous media by means of analogical and mathematical discontinous models.'' PhD thesis, Univ. Politécnica de Madrid, Spain (in Spanish).

Roelfstra, P. E. (1988). ''Numerical concrete.'' PhD thesis, Laboratoire de Matériaux de Construction, Ecole Polytéchnique Féderale de Lausanne, Lausanne, Switzerland.

Roelfstra, P. E., Sadouki, H., and Wittmann, F. H. (1985). ''Le béton numérique.'' *Mater. Struct.*, 18, 327–335.

Schlangen, E. (1995). ''Computational aspects of fracture simulations with lattice models.'' *Fracture mechanics of concrete structures (Proc., FraMCoS-2, Zürich)*, F. H. Wittmann, ed., Aedificatio, Freiburg, Germany, 913–928.

Schlangen, E. (1993). ''Experimental and numerical analysis of fracture processes in concrete.'' PhD thesis, Delft Univ. of Technology, Delft, The Netherlands.

Schlangen, E., and van Mier, J. G. M. (1992). ''Shear fracture in cementitious composites, Part II: Numerical simulations.'' *Fracture mechanics of concrete structures (Proc., FraMCoS-1)*, Z. P. Bažant, ed., Elsevier, London, 671–676.

Serrano, A. A., and Rodriguez-Ortiz, J. M. (1973). ''A contribution to the mechanics of heterogeneous granular media.'' *Proc., Symp. Plasticity and Soil Mech.*, Cambridge, U.K.

Ting, J. M., Meachum, L. R., and Rowell, J. D. (1995). ''Effect of particle shape on the strength and deformation mechanics of ellipse-shaped granular assemblage.'' *Eng. Comput.*, 12, 99–108.

van Mier, J. G. M., van Vliet, M. R. A., and Wang, T. K. (2002). ''Fracture mechanisms in particle composites: Statistical aspects in lattice type analysis.'' *Mech. Mater.*, 34(11), 705–724.

van Mier, J. G. M., Vervuurt, A., and Schlangen, E. (1994). ''Boundary and size effects in uniaxial tensile tests: A numerical and experimental study.'' *Fracture and damage in quasibrittle structures (Proc., NSF Workshop, Prague)*, Z. P. Bažant, Z. Bittnar, M. Jirásek, and J. Mazars, eds., E & FN Spon, London, 289–302.

Wittmann, F. H., Roelfstra, P. E., and Kamp, C. L. (1988). ''Drying of concrete: An application of the 3L approach.'' *Nucl. Eng. Des.*, 105, 185–198.

Zubelewicz, A. (1980). ''Contact element method.'' PhD thesis, Technical Univ. of Varsaw, Varsaw, Poland (in Polish).

Zubelewicz, A. (1983). ''Proposal of a new structural model for concrete.'' *Arch. Inzyn. Ladow.* 29, 417–429 (in Polish).

Zubelewicz, A., and Bažant, Z. P. (1987). ''Interface element modeling of fracture in aggregate composites.'' *J. Eng. Mech.*, 113(11), 1619–1630.

Zubelewicz, A., and Mróz, Z. (1983). ''Numerical simulation of rockburst processes treated as problems of dynamic instability.'' *Rock Mech. Rock Eng.*, 16, 253–274.